DMD Fast Forward. Published on March 19, 2020 as DOI: 10.1124/dmd.119.089888
This article has not been copyedited and formatted. The final version may differ from this version.



# Main manuscript

## Title Page

### Full Title

**Insights into Praziquantel metabolism and potential enantiomeric CYP-mediated drug-drug interaction**

### Authors

Gloria Vendrell-Navarro, Holger Scheible, Floriane Lignet, Howard Burt, Christian Luepfert, Andreas Marx, Nada Abla, Piet Swart, Dominique Perrin

### Affiliations

GVN, HS, FL, CL, PS, DP, AM: Merck KGaA, Darmstadt, Germany

NA: Merck Global Health Institute, Ares Trading S.A. (a subsidiary of Merck KGaA, Darmstadt, Germany), Route de Crassier 1, 1262 Eysins, Switzerland and Medicines for Malaria Venture (MMV), Geneva, Switzerland

HB: Certara UK Ltd (Simcyp Division), Sheffield, United Kingdom

Note, if required: (PS: (current) Nuvisan GmbH, Grafing, Germany)

DMD Fast Forward. Published on March 19, 2020 as DOI: 10.1124/dmd.119.089888
This article has not been copyedited and formatted. The final version may differ from this version.



## Running Title Page

### Running Title

**Praziquantel metabolism and enantiomeric CYP interactions**

### Corresponding author

Dominique Perrin

Merck KGaA

Frankfurter Str. 250 D50/225, 64293 Darmstadt, Germany.

00 49 6151 72 92217

dominique.perrin@merckgroup.com

Number of text pages: 24

Number of tables: 2

Number of figures: 7

Number of references: 30

Number of words in the Abstract: 179

Number of words in the Introduction: 488

Number of words in the Discussion: 1223

### Nonstandard abbreviations

ACN, acetonitrile; AIC, Akaike information criterion; BEH, ethylene bridged hybrid; $CL_{int}$, intrinsic clearance; $CL_{po,}$ oral clearance; CV, coefficient of variation; CYP, cytochrome P450; DDI, drug-drug interactions; DME; drug metabolizing enzymes; e.r., enantiomeric ratio; DMSO, dimethyl sulfoxide; FaSSIF, fasted state simulated intestinal fluid; $f_u$, fraction unbound; hHeps, human hepatocytes; HLM, human liver microsomes; $K_{dep}$, first-order depletion constant; $K_i$, inhibition constant; $K_m$, Michaelis constant; LC, liquid chromatography; MS/MS, Tandem mass spectrometry; n.c., non-converged; NMR, nuclear magnetic resonance spectroscopy; ODT, orally disintegrating tablet; $P_{app}$, apparent permeability; PBPK, physiologically based pharmacokinetic (modeling); PK, pharmacokinetics; PZQ, praziquantel; qTOF, Quadrupole time-of-flight mass spectrometry; rhCYP, recombinant human CYP450; SD, standard deviation; SGF, simulated gastric fluid; $V_{max}$, maximum velocity of the metabolic reaction; WHO, World Health Organisation.

DMD Fast Forward. Published on March 19, 2020 as DOI: 10.1124/dmd.119.089888
This article has not been copyedited and formatted. The final version may differ from this version.



## Abstract

The active enantiomer R-Praziquantel (PZQ) shows clinically a lower relative exposure when administered enantiomerically pure compared to a racemic form. We investigated the hypothesis that enantiomer-enantiomer interactions on CYP enzymes could explain this observation and aimed to further deepen the understanding of PZQ metabolism.

Firstly, in an in vitro metabolite profiling study, the formation of multiple metabolites per CYP, together with an observed interconversion of cis-4'-OH-PZQ to trans-4'-OH-PZQ in human hepatocytes, pointed out the inadequacy of measuring metabolite formation in kinetic studies. Thus, a substrate depletion approach to study PZQ enantiomeric interactions was applied. Secondly, an abundant CYP 3A4 metabolite found in previous studies was structurally characterized. Thirdly, substrate depletion methodologies were applied to determine CYP enzyme kinetics of PZQ and to further estimate enantiomer-enantiomer inhibitory parameters. A competitive inhibition between PZQ enantiomers for CYP2C9, 2C19, 3A4 and 3A5 was revealed. Analyses considering the clearance of only one or both enantiomers provided comparable enantiomer-enantiomer inhibition estimates. To conclude, this paper provides new insights into PZQ metabolic profile to enable a better understanding of enantioselective PK using substrate depletion-based methods.

## Significance Statement

In this study, enantiomer-enantiomer interactions of praziquantel on CYP metabolizing enzymes are investigated via substrate depletion measurement using modelling methods. Together with new insights into the praziquantel metabolism, this work provides a novel dataset to understand its pharmacokinetics.

DMD Fast Forward. Published on March 19, 2020 as DOI: 10.1124/dmd.119.089888
This article has not been copyedited and formatted. The final version may differ from this version.



## Visual Abstract

Not applicable.

## Introduction

Racemic praziquantel (PZQ) is the World Health Organisation (WHO)'s drug of choice to treat Schistosomiasis (WHO, 2009), a neglected tropical disease affecting 207 million people worldwide (WHO, 2018). Given the prevalence of this disease in young children (3 months to 6 years) (Stothard et al., 2011), the Pediatric Praziquantel Consortium (http://www.pediatricpraziquantelconsortium.org) aims to develop a pediatric formulation for this population (Bonate et al., 2018). Considering the recommendations from Research and Training in Tropical Diseases on switching to an enantiomerically pure formulation of the active form R-PZQ (WHO, 2007), one goal of the Pediatric Praziquantel Consortium was to clinically compare racemic (rac-PZQ) vs pure R-PZQ formulations (WHO, 2010), with the expectation that an enantiomeric pure formulation will result in a smaller orally disintegrating tablet (ODT) with less bitter taste, as inactive S-PZQ mainly contributes to unpleasant taste (Meyer et al., 2009). One outcome of the subsequent clinical study was that the administration of enantiomerically pure R-PZQ (20 mg/kg) resulted in 40% of relative bioavailability when compared to rac-PZQ (40 mg/kg total, containing 20 mg/kg of R-PZQ) (Bagchus et al., 2019). This could be indicative of enantiomer-enantiomer interactions and thus *in vitro* investigations were triggered. In this context, due to its complex metabolism, PZQ emerged as a case study to apply substrate depletion approaches to study metabolism-based DDI. Particularly, multiple metabolites have already been described in reactions with recombinant human CYPs (rhCYPs) and human liver microsomes (HLM), where different kinetic values have been obtained for CYP 2C9 and 3A4 depending on the metabolite measured (Wang et al., 2014). Moreover, whilst R,S-cis-4'-PZQ-OH isomers are the main metabolites in HLMs, R,S-trans-4'-PZQ-OH isomers are the most abundant metabolites in humans (Melo et al., 2005), and the mechanism behind this apparent discrepancy remains unclear to date.

Considering this background, the aim of this work was to characterize PZQ metabolism and evaluate if the lower exposure of R-PZQ when administered alone relative to an administration as Rac-PZQ could be explained by drug-drug interaction between the R and S enantiomers at the CYP level For this purpose, it was studied whether the complexity of its metabolic mechanisms makes metabolite formation

DMD Fast Forward. Published on March 19, 2020 as DOI: 10.1124/dmd.119.089888
This article has not been copyedited and formatted. The final version may differ from this version.



measurement inappropriate for kinetic profiling. The kinetic parameters ($K_m$ and $V_{max}$) for drug metabolizing enzymes (DME) are important to understand *in vitro* drug clearance and consequently, in vivo pharmacokinetics (PK) and dose-exposure relationships. Their determination is classically based on the rate of product formation at various substrate concentrations. Alternatively, monitoring of substrate depletion has been proven as an effective approach (Obach and Reed-Hagen, 2002; Nath and Atkins, 2006; Sjögren et al., 2009) when metabolite measurement becomes inappropriate, e.g. instability of metabolites or lack of standards, or for drugs presenting multiple reaction pathways leading to different Km values for a single enzyme. Moreover, this approach has notably been applied to the study of doxazosin enantiomer CYP interactions (Kong et al; 2015). Complexity of PZQ metabolism led us to use the substrate depletion method instead of metabolite formation.

## Materials and Methods

### Materials

Ultrapure water was produced from a Milli-Q® purification system (EMD Millipore, Billerica, USA) before each assay. Potassium phosphate buffer (500 mM, pH 7.4) was prepared using potassium dihydrogen phosphate and dipotassium hydrogen phosphate. These salts, as well as $MgCl_2$, were obtained from Merck KGaA (Darmstadt, Germany). Praziquantel (PZQ), R- and S-cis-4'-PZQ-OH, R- and S-trans-4'-PZQ-OH were obtained from Merck KGaA small molecule library (Darmstadt, Germany). Internal standards racemic PZQ-(cyclohexyl-$d_{11}$) (PZQ-$d_{11}$) and trans-PZQ-OH-$d_5$ were purchased from Toronto Research Chemicals (Toronto, Canada). CYP 2C19 reference substrate omeprazole was obtained from Calbiochem. Internal standard propranolol and all other reference compounds used as positive controls were obtained from Sigma Aldrich, i.e. 7-ethoxycoumarin (CYP 1A1-1A2), efavirenz (CYP 2B6), amodiaquine (CYP 2C8), diclofenac (CYP 2C9), dextromethorphan (CYP 2D6), testosterone and midazolam (CYP 3A isoforms), as well as reference substrates for hepatocyte clearance ketoprofen, naloxone and verapamil. All other reagents, solvent and chemicals were of appropriate grade and purchased from Sigma-Aldrich (Schnelldorf, Germany).

NADPH-generating system was obtained from Promega GmbH (Madison, USA). Bactosomes™ (human cytochrome P450s co-expressed with human NADPH-cytochrome P450 reductase in bacterial membrane) were purchased from Cypex Ltd (Dundee, UK). InVitroGRO™ Krebs-Henseleit buffer, thawing HT medium, pooled (mixed gender) (HLM) and human cryopreserved hepatocytes (hHep) were obtained from BioreclamationIVT (Baltimore, USA).

DMD Fast Forward. Published on March 19, 2020 as DOI: 10.1124/dmd.119.089888
This article has not been copyedited and formatted. The final version may differ from this version.



**rhCYPs incubations with PZQ**

All incubations were performed in 96-well conical bottom plates (0.3 mL) in a Thermomixer (Eppendorf AG, Hamburg, Germany) at 37°C under stirring conditions. Reactions were run in duplicate (intra-assay n=2), and at least 2 inter-assay replicates (N) were performed. NADPH-generating system (final 1.3 mM NADP, 3.3 mM glucose-6-phosphate, 3.3 mM $MgCl_2$, and 0.4 U/ml glucose-6-phosphate dehydrogenase) in potassium phosphate buffer (final 100 mM, pH 7.4) was pre-warmed for 5 min at 37°C (60 µL/well). Dimethyl sulfoxide (DMSO) intermediate solutions of substrates (500X) were prepared and diluted 1:250 in 37 °C pre-warmed water to obtain a 2X working solution, which was added to the to pre-warmed NADPH-containing solution (75 µL/well). After 5 min of pre-incubation, pre-warmed rhCYPs (10X, 15 µL/well) were added to start the incubation, which had a total volume of 150 µL and contained 0.2% (v/v) DMSO. rhCYP 1A2, 2B6, 2C8, 2C9, 2C19, 2D6, 3A4, 3A5 and 3A7 were used in PZQ incubations at a concentration of 50 pmol CYP/mL. rhCYP 1A1 and rhCYP 2C19 were used at 17.5 and 20 pmol CYP/mL, respectively, due to faster turnover. Reaction monitoring was conducted under initial linear rate conditions (typically 0 - 30 min) by quenching aliquots into an ice-cold solution (100 µL) containing internal standards (65/35 (v/v) acetonitrile (ACN)/water, 300 nM propranolol, 60 nM PZQ-$d_{11}$). After centrifugation (4000 g, 50 min, 4°C), supernatants were diluted prior to analysis by LC-MS/MS, ensuring the same final proportion of 25% (v/v) ACN for all samples. Calibration standard samples were prepared using a matrix consistent with experimental samples and were equally diluted.

R-PZQ, S-PZQ and rac-PZQ were tested at 1.0 µM for CLint determination (N=3). Initial tests were performed to determine reaction linearity and protein binding effects. For the determination of the kinetic parameters, 10 concentrations log-scale distributed over a concentration range of 200-0.01 µM were used (N=2). Based on initial linearity experiments, measured time points were adjusted for rhCYP 1A2, 2C9, 2D6, 3A4, 3A5 to 0-5-10-20-30 min, for rhCYP 1A1 and 2C19 to 0-4-8-16-24 min; and for rhCYP 3A7 to 0-5-10-20-30-50-75 min. A selection of samples (1 and 10 µM, 0 and 30 min) were analyzed by LC-qTOF for metabolite profiling. For $K_i$ determination, R-PZQ and S-PZQ were incubated with selected rhCYPs in a 7 x 7 matrix ratio (N=2), at concentrations equivalent to 5, 2, 0.8, 0.32, 0.12, 0.05 and 0 $K_m$ values (where 0 $K_m$ are incubations with “substrate enantiomer” in the absence of “inhibitory enantiomer”). Parallel incubations with specific reference compounds for each CYP isoform were used as positive controls (1 µM, n=2), i.e. 7-ethoxycoumarin for CYP 1A1/2, efavirenz for CYP 2B6, amodiaquine for CYP 2C8, diclofenac for CYP 2C9, omeprazole for CYP 2C19, dextromethorphan for

DMD Fast Forward. Published on March 19, 2020 as DOI: 10.1124/dmd.119.089888
This article has not been copyedited and formatted. The final version may differ from this version.



CYP 2D6, testosterone and midazolam for CYP 3A4/5/7. Negative control was carried out using membrane protein isolated from *E. coli* host strain.

**Microsomal incubations for PZQ metabolite profiling**

R-PZQ, S-PZQ and rac-PZQ (final 1 and 10 µM) were dissolved in 4.5 mL of 100 mM potassium phosphate buffer with 1.0 mM $MgCl_2$ in 15 mL glass tubes and mixed in addition of the respective HLM (1 mg/mL). Incubations (37°C, 150 rpm) were started by pipetting a 2 mL aliquot of this mixture in a new vial and adding 200 µL of 20 mM NADPH solution and were terminated at t timepoints 0, 15, 30 and 60 min by quenching in ice-cold ACN. Control incubations with buffer were performed in parallel.

**Hepatocyte incubations with PZQ and its metabolites**

For metabolite identification purposes, R-PZQ, S-PZQ and rac-PZQ were used at a final concentration of 1 and 10 µM. For metabolite interconversion studies, compounds were tested at a final concentration of 5 µM and 10 µM, except for M6 (estimated concentration 2.5 µM), and at least 2 inter-assay replicates were performed (N≥2). Stock solutions of selected compounds were spiked into Krebs-Henseleit buffer to lead to a 2X solution and pre-warmed in small 1.5 mL centrifuge tubes with a Thermomixer at 37°C and 450 rpm. hHeps were thawed and plated in a 24-round well plate (final 2 × 10e6 cell/mL, 450 µL/well) according to the manufacturer's protocol. Reactions were initiated by addition of prewarmed compound (1:1, 450 µL/well) to hHeps (37°C), incubated under stirring conditions (37°C, 5% $CO_2$, 100 rpm). Aliquots were collected over time up to 180 minand were terminated by quenching in ice-cold ACN. Control incubations with buffer and reference substrates ketoprofen, naloxone and verapamil were performed in parallel.

**Production of PZQ metabolite M6**

M6 was produced by a scale-up reaction of each PZQ enantiomer (125 nmol) with rhCYP3A4 (1.37 nmol CYP) in a total of 25 mL of potassium phosphate buffer (100 mM, pH 7.4) containing NADPH (1.2 mM) and 3.3 mM $MgCl_2$. Reaction was performed as described previously and quenched after 40 min by addition into ice-cold ACN (37.5 mL total). After centrifugation to remove pellet, supernatant was concentrated. Semi-preparative high-performance LC (HPLC) was carried out on a Hitachi L-6200 pump equipped with a Hitachi L-4200 UV-VIS detector (Tokyo, Japan); equipped with a column Chromolith Performance RP-18e (monolithic, 4.6 × 100 mm) (Merck Millipore, Darmstadt, Germany) and using as

DMD Fast Forward. Published on March 19, 2020 as DOI: 10.1124/dmd.119.089888
This article has not been copyedited and formatted. The final version may differ from this version.



mobile phases were (A) water and (B) ACN. Purification was performed at room temperature at a flow rate of 1 mL/min, applying a multi-segmented gradient from 0–25% B in 7 min, 25–30% B in 3 min, 30-55% B in 5 min, 55–80% B in 5 min and 80% B for 5 min, where M6 was detected and concentrated. Estimated final purity was > 95% (HPLC-UV).

**Instrumentation and analysis**

Quantitative LC-MS/MS analysis

Waters Acquity LC system consisted of a Waters Acquity binary solvent manager, column manager and autosampler set up at 15°C (Waters, Eschborn, Germany). The mobile phases were (A) ammonium formate (10 mM) with 0.1% formic acid and (B) ACN with 0.1% formic acid. Waters Acquity Ethylene Bridged Hybrid (BEH) C18 column (1.7 µm, 2.1 × 50 mm) equipped with a Waters Acquity UPLC® BEH C18 pre-column (1.7 µm, 2.1 × 5 mm) was used for non-chiral separations at 40°C, whereas Phenomenex Lux Cellulose-2 column (3 µm, 2 × 150 mm) (Phenomenex, Torrance, USA) equipped with a Phenomenex Lux Cellulose-2 pre-column (3 mm ID) at 22°C was used for chiral separations. Mass spectrometry was performed with a quadrupole ion trap (QTRAP) 5500 mass spectrometer (AB Sciex, Darmstadt, Germany). Instrument control, data acquisition, and evaluation were performed using Applied Biosystems/MDS Sciex™ Analyst software version 1.6.3 (AB Sciex, Darmstadt, Germany). Analyte concentration was calculated by interpolating relative peak area to internal standard peak area on the corresponding calibration curve set. If needed, concentrations tested per each assay were grouped, and each group was diluted and analyzed using different calibration standard curves equally treated to be within MS/MS linear dynamic range. Non-chiral analysis of (R,S)-PZQ and (R,S)-M6 was performed using BEH C18 column and applying a linear gradient method at a flow of 0.7 mL/min of 0% B isocratic for 0.1 min, 0% to 100% B in 1.14 min, 100% B for 0.3 min and 0% B for 0.5 min. For chiral analysis of (R,S)-PZQ and (R,S)-M6, Phenomenex Lux column was employed and isocratic conditions at a flow of 0.45 mL/min were used: 85% B for 4.0 min, 100% B for 1.8 min and 85% B for 1.2 min. Chiral analysis of all 4'-OH-PZQ metabolites was performed with Phenomenex Lux column using (A) water with 0.1% formic acid and (B) ACN with 0.1% formic acid at a flow of 0.36 mL/min and isocratic conditions of 36% B for 6.0 min, followed by a wash with 100% B for 3.0 min. LC effluent was introduced into the mass spectrometer in positive ion mode, having entrance potential at 10 V and ion spray temperature at 600°C. The multiple reaction monitoring transitions of the precursor ions $(M + H)^+$ to the corresponding product ions were m/z 313.2 to 203.2 for PZQ, 329.16 to 203.25 for (R,S)-(cis,trans)-4'-

DMD Fast Forward. Published on March 19, 2020 as DOI: 10.1124/dmd.119.089888
This article has not been copyedited and formatted. The final version may differ from this version.



OH-PZQ metabolites, 329.16 to 311.08 for (R,S)-M6. Following transitions were used for internal standards: 324.2 to 204.0 for PZQ-d11, 334.307 to 132.053 for trans-4'-OH-PZQ-d5, 260.2 to 183.1 for propranolol.

**Metabolite profiling by LC-qTOF**

Metabolite separation was performed on a Waters Acquity UPLC® system, consisting on a Waters Acquity binary solvent manager, column manager, photodiode array detector and autosampler set up at 10°C coupled to a Xevo G2-S qTOF mass spectrometer (all from Waters, Eschborn, Germany) operated in electrospray ionization (ESI) positive mode. Metabolite identification was performed on a Waters UPLC® HSS T3 column (1.8 µm, 100 × 2.1 mm) using eluent A (water + 0.1% formic acid) and eluent B (ACN + 0.1% formic acid) with a linear gradient at a flow of 0.6 mL/min starting with 2% eluent B until 0.5 min then changing to 25% B at 2.4 min, 30% B at 3.3 min, 65% B at 6.6 min, 95% at 6.7 min and equilibrating back at 2% B until 14.1 min. Metabolite identification was supported by UNIFI version 1.8.2 (Waters, Eschborn, Germany) and MassMetasite/WebMetabase version 3.3 (Molecular Discovery, Perugia, Italy).

**Structural elucidation of PZQ metabolite M6**

NMR of purified M6 was performed at 298 K on a 700 MHz Bruker Avance III equipped with a 5 mm cryocooled triple resonance probe (TCI). All samples were dissolved in DMSO-$d_6$. $^1$H NMR spectra were acquired with 64 k time domain points, a spectral width of 20 ppm, a relaxation delay of 10 s and 256 scans. Water suppression was achieved by pre-saturation of the water signal at 3.3 ppm using the Bruker *zgpr* standard pulse sequence. Edited heteronuclear single quantum coherence (HSQC) NMR spectra were acquired with 1024 × 256 time domain data points over a spectral width of 12ppm in the *t2* and 165 ppm in the *t1* dimension. Homonuclear correlation spectroscopy (COSY) NMR spectra were acquired with 1024 × 256 time domain data points over a spectral width of 12 ppm in the *t2* and *t1* dimension.

**Data Analysis**

A detailed overview of the kinetic parameters analyzed with abbreviations and units is given on Table S7.

***In vitro* enzyme kinetics based on substrate depletion**

DMD Fast Forward. Published on March 19, 2020 as DOI: 10.1124/dmd.119.089888
This article has not been copyedited and formatted. The final version may differ from this version.



Substrate saturation data were analyzed using GraphPad Prism version 6.05 and higher (GraphPad Software, La Jolla, CA USA). Using substrate concentrations (S, in µM) over time (t, in min), first-order depletion constant ($k_{dep,}$ in $min^{-1}$) based on remaining compound (in %) was calculated with equation (1) and further used to determine the intrinsic clearance ($CL_{int}$) at 1.0 µM using equation (2) and considering CYP concentration ($C_{rhCYP}$).

$$[S]_t = [S]_0 \times e^{-k_{dep} \times t} \quad (1)$$

$$CL_{int} = \frac{k_{dep}}{C_{rhCYP}} \quad (2)$$

For intrinsic clearance measurements at a single concentration, CYP concentration was expressed in (pmol CYP/µL) to give $CL_{int}$ values in µL/min/pmol CYP. The threshold of relevance was calculated considering < 75% remaining compound after incubation time. Propagated intra-assay and inter-assay variations (SD, CV) were calculated.

The enzyme kinetic parameters were determined by the multiple substrate depletion curves method (Obach RS and Reed-Hagen AE, 2002; Sjögren et al., 2009), using as basis the nonlinear regression defined by Nath and Atkins, 2006 in equation (3), where $K_m$ (in µM, i.e. µmol substrate/L) is the Michaelis constant, $\nu_{max}$ (in µmol substrate/L/min) is the maximum depletion rate not normalized to rhCYP concentration, and thus $\nu_{max}/K_m$ (in $min^{-1}$) equals to the theoretical maximum consumption rate constant at an infinitesimally low substrate concentration, i.e. $k_{dep(S=0)} \sim k_{dep(\infty)}$. Michaelis-Menten $V_{max}$ is obtained by dividing $\nu_{max}$ with rhCYP concentration ($C_{rhCYP}$) (as nmol CYP/L), which is further converted to the desired units (pmol/pmol CYP/min) by multiplying the result per 1000.

$$k_{dep} = \left(\frac{v_{max}}{K_m}\right) \times \left[1 - \left(\frac{[S]}{K_m + [S]}\right)\right] \quad (3)$$

$k_{dep}$ were determined for each concentration considering only log-linear time range of disappearance. At least 4 time points in 8 different substrate initial concentrations were selected. This dataset was used to plot $k_{dep}$ versus the initial substrate concentration into the sigmoidal-like curve described in equation (3). Propagated intra-assay and inter-assay variations (SD, CV) were considered to flag the data as not converged. Standard error of mean (which considers intra- and inter-assay variability) was used for graphical representations.

**Linear static modeling for the determination of inhibition constants based on substrate depletion**

DMD Fast Forward. Published on March 19, 2020 as DOI: 10.1124/dmd.119.089888
This article has not been copyedited and formatted. The final version may differ from this version.



Equation (3) was used as basis to define different inhibition models. Competitive inhibition was described by including an observed $K_m$ ($K_{m,obs}$, in µM) described in equation (4), where [I] is the inhibitor concentration (in µM) and $K_i$ the inhibition constant (in µM).

$$K_{m,obs} = K_m \times \left(\frac{1+[I]}{K_i}\right) \quad (4)$$

Leading to a modified equation (3) for competitive inhibition as described in equation (5):

$$k_{dep} = \left(\frac{v_{max}}{K_m \times \left(\frac{1+[I]}{K_i}\right)}\right) \times \left[1 - \left(\frac{[S]}{\left(K_m \times \left(\frac{1+[I]}{K_i}\right)\right) + [S]}\right)\right] \quad (5)$$

Non-competitive inhibition included the concept of an inhibited $\nu_{max}$ ($\nu_{max,inh}$) as described in equation (6).

$$v_{max,inh} = \frac{v_{max}}{\left(\frac{1+[I]}{K_i}\right)} \quad (6)$$

Leading to a modified equation (3) for non-competitive inhibition as described in equation (7)

$$k_{dep} = \left(\frac{v_{max}}{K_m \times \left(\frac{1+[I]}{K_i}\right)}\right) \times \left[1 - \left(\frac{[S]}{K_m + [S]}\right)\right] \quad (7)$$

The different nonlinear regression inhibitory equations were fitted to log-linear substrate data and Akaike's Information Criteria (AIC) was used to diagnose which inhibition type fitted better. Propagated intra-assay (n=2) and inter-assay (N=2) standard deviations were obtained.

Linear-mixed inhibition was described with a simplified model by introducing apparent $\nu_{max}$ and $K_m$ concepts described with the alpha constant (dimensionless), which is an indicator of the inhibition mechanism:

$$v_{max,app} = \frac{v_{max}}{\left(\frac{1+[I]}{\alpha \times K_i}\right)} \quad (8)$$

$$K_{m,app} = K_m \times \left(\frac{1+\frac{[I]}{K_i}}{1+\frac{[I]}{\alpha \times K_i}}\right) \quad (9)$$

**Non-linear dynamic modeling for the determination of inhibition constants based on substrate depletion**

Dynamic models were developed using the software Phoenix Winnonlin 6.4, NLME 1.3 (Certara, L.P, Princeton, New Jersey). Competitive and non-competitive inhibition models were defined. In those models, the concurring kinetics of R-PZQ and S-PZQ were defined by the set of differential equations

DMD Fast Forward. Published on March 19, 2020 as DOI: 10.1124/dmd.119.089888
This article has not been copyedited and formatted. The final version may differ from this version.



(10) and (11), where the parameters are expressed as previously, i.e. time (t, in min, $k_{dep}$ in $min^{-1}$ and substrate concentration (i.e. R_PZQ and S_PZQ) in µM.

$$\frac{d\ R\_PZQ}{dt} = -k_{dep,S\_PZQ} * R\_PZQ \quad (10)$$

$$\frac{d\ S\_PZQ}{dt} = -k_{dep,R\_PZQ} * S\_PZQ \quad (11)$$

In the competitive model, for each enantiomer an observed $K_m$ term ($K_{m,obs}$) (source equation (4)) was integrated to the expression of $k_{dep}$ as defined respectively in equations (4) and (5), with the difference that the inhibitor concentration used for the calculation of the term $K_{m,obs}$ was not the initial concentration of the competing enantiomer, but its time-dependent concentration.

Similarly for a non-competitive model, for each enantiomer a term $\nu_{max,inh}$ was integrated to the expression of $k_{dep}$ as defined respectively in equations (6) and (7), where the inhibitor concentration used for the calculation of the term $\nu_{max}$ was not the initial concentration of the competing enantiomer, but its time-dependent concentration.

The kinetic parameters were estimated for each CYP by fitting the two differential equations (10 and 11) to the R- and S-PZQ concentrations measured in the inhibition experiments, using a quasi-Newton optimization algorithm minimizing the negative log-likelihood implemented in the modelling software. Complete sets of equations can be found in the supplementary material (Table S8).

## Results

### Metabolite identification of PZQ enantiomers

Metabolite profiling and identification of single PZQ enantiomers and PZQ racemate in incubations with recombinant human CYP enzymes (i.e. CYP 1A1, 1A2, 2B6, 2C8, 2C9, 2C19, 2D6, 3A4, 3A5, and 3A7), human liver microsomes (HLM) and hepatocytes (hHeps) revealed in total six mono-oxidized metabolites (see Figure 1-2 and Table S1-S2) and several further secondary oxidative metabolites (+32 Da and +14 Da) (data not shown). This is in line with the already published data (Huang et al., 2010; Wang et al., 2014). From the mass spectrometric elucidation, oxidation to metabolites M1, M5 and M6 could be allocated to the “core moiety” (i.e. hexahydro-pyrazino[2,1-a]isoquinolin-4-one ring system), whereas all other metabolites (M2 = trans-4‘-OH-PZQ, M4 = cis-4‘-OH-PZQ, and M3 = exact structure unknown) could be assigned to an oxidation on the cyclohexane ring (Figure 1, Table S1-S2). Comparison of the mono-oxidation metabolites formed in the different test systems (Figure 2) indicated that hHeps are the biological system where trans-4‘-OH-PZQ becomes the major isomer instead of cis-

DMD Fast Forward. Published on March 19, 2020 as DOI: 10.1124/dmd.119.089888
This article has not been copyedited and formatted. The final version may differ from this version.



4'-OH-PZQ. Metabolite identification in incubation of racemic-PZQ was performed, which confirmed the findings of the enantiopure PZQ incubations (data not shown). Moreover, given its relative abundance in CYP3A incubations, M6 was further isolated from scaled-up incubation of both R- and S-PZQ with CYP3A4 and characterized by NMR analysis (Figure S1-S4), which confirmed to correspond to the structure M6 shown in Figure 1. R- and S-M6 spectra were identical by NMR (Figure S4). Attempts to distinguish both products via enantioselective HPLC were inconclusive. NMR structural elucidation of M6 resulted on the following signal assignment: $^{1}$H NMR (700 MHz, DMSO-$d_6$) δ 7.62 (d, $J$ = 7.6 Hz, 1H), 7.38 – 7.27 (m, 3H), 7.23 (d, $J$ = 6.7 Hz, 1H), 4.61 (d, $J$ = 18.1 Hz, 1H), 4.58 – 4.51 (m, 1H), 4.41 (d, $J$ = 13.2 Hz, 1H), 3.62 (d, $J$ = 18.1 Hz, 1H), 3.38 (d, $J$ = 13.6 Hz, 1H), 3.07 – 2.97 (m, 1H), 2.89 – 2.81 (m, 1H), 2.81 – 2.70 (m, 2H), 1.77 – 1.61 (m, 4H), 1.47 – 1.12 (m, 6H).

**Metabolite interconversion in human hepatocytes**

The metabolic stability of PZQ and selected metabolites, i.e. trans-4'-OH-PZQ (M2), cis-4'-OH-PZQ (M4), and M6 metabolites from both R- and S-PZQ, was further studied in hHep incubations. R-PZQ and S-PZQ presented a similar clearance at 5-10 µM (19 and 16 µL/min/10e6 cells, respectively), and no chiral inversion was observed. Incubations of PZQ metabolites with hHeps revealed an interconversion of R-cis-4'-OH-PZQ to R-trans-4'-OH-PZQ, and to a lower extent from S-cis-4'-OH-PZQ to S-trans-4'-OH-PZQ (Figure 3), which was not observed in any control or other test system. Clearance of R-cis-4'-OH-PZQ (8 µL/min/10e6 cells) was comparable to the clearance of parent R-PZQ, and R-trans-4'-OH-PZQ formation rate from R-cis-4'-OH-PZQ (29 pmol/min/10e6 cell) was 3-fold higher in comparison to formation from parent R-PZQ (9 pmol/min/10e6 cell) (Table S3). This finding could be dueto the presence of a non-microsomal enzyme, which could then partially explain why R-trans-4'-OH-PZQ is a major metabolite in hepatocytes and in-vivo, but not in HLM or rhCYPs. Hepatocyte incubations of S-cis-4'-OH-PZQ result on a lower clearance (3 µL/min/10e6 cells) in comparison to parent S-PZQ, and lead to the formation of S-trans-4'-OH-PZQ (formation rate 6 pmol/min/10e6 cell), which is similar to S-cis-4'-OH-PZQ formation rate starting from S-PZQ (4 pmol/min/10e6 cell). Overall, a net increase of S-cis-4'-OH-PZQ from S-PZQ can be observed in hepatocytes at incubation times from 30 min via 90 min to 180 min, whereas R-cis-4'-OH-PZQ level from R-PZQ incubations decreases between 90 min and 180 min time points, as shown in Figure 2.

DMD Fast Forward. Published on March 19, 2020 as DOI: 10.1124/dmd.119.089888
This article has not been copyedited and formatted. The final version may differ from this version.



Lack of exact analytical standards for M6 hampered its quantification. Nevertheless, M6 stability in hHeps was qualitatively evaluated and a concentration decrease over time was found (5 µL/min/10e6 cells), which could explain its very low abundance in hHep incubations with parent PZQ.

**Time-dependent turnover of PZQ in rhCYPs**

To determine the role of human CYP enzymes involved in the metabolic clearance of PZQ, single enantiomers and racemate were incubated with a panel of rhCYP enzymes, i.e. CYP 1A1, 1A2, 2B6, 2C8, 2C9, 2C19, 2D6, 3A4, 3A5, and 3A7. Protein binding effect was negligible as demonstrated by control membrane incubations and time-course experiments at different protein concentrations (data not shown), thus an adjustment for unbound concentrations and clearance was not needed (Sjögren et al., 2009).

A relevant turnover was observed for all CYPs except CYP 2B6 and 2C8. Comparison of the clearance values between PZQ enantiomers tested at 1.0 µM as single enantiomer (i.e. 100% e.r.) indicated a similar efficiency in metabolizing both enantiomers for CYP 2C19, 3A4 and 3A5. Relevant differences were found for the other CYP isoforms, i.e. R-PZQ is a preferred substrate over S-PZQ for CYP 1A1, 1A2, 2C9 and 2D6, whereas S-PZQ is preferred over R-PZQ for CYP 3A7 (Figure 1, Table S4). By inspecting the catalytic efficiency of the different CYP isoforms, the highest clearance values were found for CYP 2C19 metabolizing both enantiomers, as well as for CYP 1A1 metabolizing R-PZQ. Clearance values of PZQ enantiomers individually tested at 1.0 µM (i.e. 100% e.r.) and evaluated by reverse phase LC-MS/MS were similar to the clearance values of each PZQ enantiomer tested in a 1.0 µM racemic mixture (i.e. 50% e.r.) and analyzed by enantioselective LC-MS/MS, i.e. below 2-fold difference (Figure 4, Figure S5 and Table S5). This is considered within normal experimental variability, thus indicating that methodological differences did not result in systematic deviations.

**Determination of kinetic values of PZQ enantiomers for CYP enzymes based on substrate depletion**

Kinetic differences between PZQ enantiomers were studied by means of evaluating $K_m$ and $V_{max}$ parameters of each enantiomer, either tested single or as racemate, for CYP isoforms presenting relevant *in vitro* contribution to the PZQ metabolism (i.e. CYP 1A1, 1A2, 2C9, 2C19, 2D6, 3A4, 3A5 and 3A7). Michaelis-Menten parameters were determined based on substrate depletion (Obach RS and Reed-Hagen AE, 2002) in order to consider overall metabolism conducted by each enzyme if multiple

DMD Fast Forward. Published on March 19, 2020 as DOI: 10.1124/dmd.119.089888
This article has not been copyedited and formatted. The final version may differ from this version.



substrate positions are oxidized. Following this approach, relevant differences (> 2-fold) on kinetic parameters between PZQ enantiomers were found (Table S6). Higher affinity for R-PZQ over S-PZQ was observed for CYP 1A1/1A2, whereas CYP 2C19 presented lower $K_m$ value for S-PZQ (Figure 5). Maximum turnover rate ($V_{max}$) was higher for R-PZQ in CYP 2C9 and 2C19, whereas $V_{max}$ of S-PZQ was greater when cleared by CYP 1A1 (Figure 6). Of note, the estimation of kinetic parameters for low clearance enzymes had high standard deviations associated and thus are not discussed here (e.g. CYP 2D6). For those cases, metabolism rate was low and did not increase at low substrate concentrations, resulting in sigmoidal curves tending to flatness.

The kinetic parameters were determined as well in the racemic mixture, to indicate if enantiomer-enantiomer interactions occurred for any CYP, which can be suspected if kinetic parameters of individually tested enantiomers (i.e. 100% e.r.) are different from tested as racemate (i.e. 50% e.r.) (Table S6). In order to visualize the relevance of those differences, a correlation analysis was performed (Figure S6a,b). A relevant increase in the affinity (> 2-fold decrease of $K_m$) and decrease in the turnover rate (> 2-fold decrease of $V_{max}$) of one enantiomer in the presence of the other one was observed for S-PZQ by CYP 1A1, R-PZQ for 2C19 as well as for both enantiomers for CYP 2C9. CYP 3A5 presented similar behavior, although $V_{max}$ fold change (1.9) was just below limits. Contrarily, an apparent affinity decrease (increased $K_m$) and $V_{max}$ increase was observed for S-PZQ by CYP 3A7 in the presence of R-PZQ. Those differences between enantiomers individually tested (100% e.r.) or in a racemate (50% e.r.) did not result in a net change in the catalytic efficiency ($V_{max}/K_m$ ratio) and did not differ from the clearance value found at 1.0 µM (< 1.5-fold difference), indicating that those potential interactions were competitive in nature (Figure S6c,d).

Comparing our substrate depletion-based $K_m$ dataset (Table S6) with metabolite formation-based values using rhCYPs by Wang (Wang et al., 2014), whereas similar values were found for CYP 2C9 (Wang metabolite IV), our CYP 3A4 values were 6-fold and 2-fold lower for R-PZQ and S-PZQ, respectively, than following Wang's metabolite VII formation. Additionally, a mean $K_m$ of R- and S-PZQ enantiomers tested as racemate was calculated, to compare it with Li's studies on rac-PZQ in rhCYPs following metabolite formation (Li et al., 2003). By means of cis-4'-OH-PZQ formation, our $K_m$ for CYP 1A2 and 2C19 were 2.1 and 3.3-fold lower, respectively. By means of Li's "X-OH-PZQ" formation (potentially our M6), our $K_m$ for CYP 3A4 was 4-fold lower. This could be a consequence of accounting for all reactions

DMD Fast Forward. Published on March 19, 2020 as DOI: 10.1124/dmd.119.089888
This article has not been copyedited and formatted. The final version may differ from this version.



occurring with the same CYP instead of just one. As seen in Figure 1, the relative amount of diverse PZQ metabolites generated for each CYP indicate that these multiple pathways might not be negligible.

**Determination of enantiomer-enantiomer interactions**

Generally, if enantiomer-enantiomer inhibition occurs, one enantiomer will play mainly a victim role (namely substrate) and the other one the perpetrator (inhibitor). In order to determine the inhibition type and estimate the inhibitory constants, two approaches were postulated. The first approach consisted in simplified static modeling where the metabolism of the inhibitor is not considered, which is based on linear regression calculations and thus it can be addressed with simple curve fitting software (e.g. Graphpad Prism). The second approach considered the metabolism of all substances involved, thus requiring non-linear regression analysis tools.

Based on Michaelis-Menten from equation (3) and the classical inhibition equations (4) and (6), formulas were derived for the competitive inhibition (equation (5)), non-competitive inhibition (equation (7)) and linear-mixed mechanisms by means of substrate depletion rate (equation (8) and (9)). The linear static approach makes a direct use of these equations, considering that the inhibitor concentration parameter remains constant over time. The non-linear dynamic approach based on equations (10) and (11) considers both substrate and inhibitor concentration as variables over time, coming in equations (4) and (5) for the competitive inhibition and equation (6) and (7) for the non-competitive inhibition. Given the relatively moderate fraction unbound of PZQ in plasma (20%, Table S10) and the observed linear monoexponential decay of its metabolism, fraction unbound and changes in the enzymatic activity over time (Jones and Houston, 2004; Sjögren et al., 2009) were considered negligible and were not included in the equations.

Generally, it is important to work under initial rate conditions with substrate depletion approaches (Nath and Atkins, 2006). Given the assumptions of the linear static model, this requisite becomes more critical for this model. It is expected that the inhibitory parameters can be determined with more confidence for those cases where substrate turnover is faster metabolized and inhibitor disappearance over time is negligible. For those cases where both compounds are metabolized with similar efficiency, the linear static model is expected to result in poor quality estimates.

DMD Fast Forward. Published on March 19, 2020 as DOI: 10.1124/dmd.119.089888
This article has not been copyedited and formatted. The final version may differ from this version.



In this study, enantiomer-enantiomer interaction experiments were conducted by varying both R- and S-PZQ initial concentrations. Concentration ranges were narrowed in comparison to those chosen for the determination of kinetic values, due to bioanalytical limitations of measuring simultaneously two analytes at different concentration ranges. Thus, a concentration range was chosen to capture the expected sigmoidal shape at the expense of including limited plateau areas. This is exemplified in Figure 7 with the interaction study on CYP 2C19 metabolism. Assays were performed in selected rhCYPs where an interaction was suspected from previous kinetic comparison of PZQ enantiomers tested individually or in a racemate.

Firstly, PZQ enantiomer-enantiomer interactions were investigated by means of linear static models of interaction (Table 1, Table S8). $K_m$ and $V_{max}$ values obtained were comparable to those found in kinetic experiments with single PZQ enantiomers (100% e.r.) (< 2-fold difference), with the exception of S-PZQ metabolized by CYP 2C19 (2.4-fold higher $K_m$ and 2.6-fold higher $V_{max}$ with linear static model), and R,S-PZQ metabolism by CYP 3A5 ($K_m$ and $V_{max}$ values were > 2.5 fold lower with linear static model). The good correlation between kinetic values of single PZQ enantiomers and kinetic values using inhibition linear static modeling demonstrated that tightening the concentration range did not impact the calculation of the inhibition parameters. However, lower and upper flat areas of the kinetic curves become critical for low clearance instances, where it is difficult to distinguish the sigmoidal pattern. As a result, the estimation of CYP 1A1 (for S-PZQ) and 3A7 (for R,S-PZQ) interaction parameters resulted in an unreliable fit with both linear static and non-linear dynamic models. When looking at $K_i$ values, competitive model fitted data better than non-competitive and linear-mixed model for 2C9, 2C19, 3A4 and 3A5, i.e. the mean probability that a competitive model was correct in comparison to a non-competitive model by means of AICc was > 75% (Ludden et al., 1994). This can be as well concluded from the similarity between $K_m$ and $K_i$ values. PZQ enantiomer interaction on CYP 1A1 presented some non-competitive character for R-PZQ as inhibitor (mean probability competitive *vs* non-competitive by AIC below 55%), finding a $K_i$ 8-fold higher than its $K_m$ value (Table S9).

With this apparent mixed inhibition character, a linear mixed inhibition model was attempted for CYP 1A1. Same $K_m$, $V_{max}$ and $K_i$ values as for competitive model were found, and with large alpha values ($\alpha$ > 30) associated, which could indicate mostly a competitive interaction (see equation 8 and 9). Linear mixed model gave also similar kinetics estimates to competitive model (< 2-fold difference) for other

DMD Fast Forward. Published on March 19, 2020 as DOI: 10.1124/dmd.119.089888
This article has not been copyedited and formatted. The final version may differ from this version.



CYPs and with large alpha values too. However, high variability ($CV_{intra}$ > 80%) was associated to alpha values (data not shown), which makes the linear-mixed model overall inconclusive.

Secondly, non-linear dynamic models (competitive and non-competitive) were fitted to the same experimental data (Table 1, Table S9). By comparing the non-linear dynamic inhibition dataset with the kinetic values with single PZQ enantiomers, similar discrepancies were found as with the linear static model, i.e. > 2-fold higher $K_m$ and $V_{max}$ values were found for S-PZQ metabolized by CYP 2C19 and for R,S-PZQ metabolized by CYP 3A5. In addition, $K_m$ and $V_{max}$ estimates of CYP 1A1 for S-PZQ were > 2-fold lower than the $K_m$ and $V_{max}$ values of single PZQ enantiomers (i.e. 100% e.r.), approaching values found for each enantiomer in a racemate (i.e. 50% e.r). (Table S9). $K_i$ values of PZQ enantiomer interactions on CYP 2C9, 2C19, 3A4 and 3A5 mediated-metabolism were well described by a competitive model as well. For CYP 1A1, although a non-competitive model could not satisfactorily be fitted to the experimental data, a non-competitive character can be suspected as $K_i$ for R-PZQ was 3.3-fold higher than $K_m$ by using this non-linear approach.

Overall, linear static and non-linear dynamic modelling yield similar results, but the non-linear dynamic model provided tighter inter-assay variability (i.e. SD on $K_m$, $V_{max}$ and $K_i$ values were at least 1.5-fold lower in 67% of the cases). This gives an indication that integrating metabolism of both compounds involved in the interaction might help to improve estimates. $K_i$ ratios between PZQ enantiomers were calculated for both static and dynamic approaches, finding similar results as well. From this analysis, it was notable that S-PZQ had a lower $K_i$ value compared to R-PZQ for CYP 2C19 (2.3-fold lower for static model and 3.9-fold lower for dynamic model), pointing out that in this case, S-PZQ might act as perpetrator of R-PZQ metabolism.

DMD Fast Forward. Published on March 19, 2020 as DOI: 10.1124/dmd.119.089888
This article has not been copyedited and formatted. The final version may differ from this version.



## Discussion

In order to investigate the PZQ enantioselective pharmacokinetic behavior previously hypothesized (Bagchus et al., 2019), selected aspects of its *in vitro* metabolism were explored. First, metabolite identification in *in vitro* systems of increasing biological complexity was addressed, i.e. rhCYPs, HLM and hHeps. Beyond confirming previous metabolite profiling of PZQ (Huang et al., 2010; Wang et al., 2014), the structure of M6, a major product in rhCYP3A4 and HLM, was finally elucidated, pointing unequivocally to the carbon-11b in the "core moiety" of PZQ as the hydroxylation site (Figure 1). M6 might correspond to a metabolite postulated in previous studies (Nleya et al., 2019). We have demonstrated that M6 is present at low abundance in hHeps and is being cleared in this *in vitro* system. However, the DME inhibitor potential of M6 remains to be explored, in order to evaluate whether it may have an impact on overall PZQ pharmacokinetics. Other known mono-oxidation metabolites found in rhCYP incubations correlated quite well with their relative abundance in HLM considering CYP expression, thus no major contributions from other CYPs were expected. However, a clear switch in the metabolite profile occurred going from HLM to hHeps, where trans-4'-OH-PZQ became the major metabolite (Figure 2). In this sense, we have identified that R-cis-4'-OH-PZQ, and to a minor extend S-cis-4'-OH-PZQ, are interconverted to the corresponding trans isomers in hHeps (Figure 3). We speculate that this reaction might be driven enzymatically via a non-CYP system, given that this interconversion only occurs in hHeps. Further studies are warranted to identify its underlying mechanism and reaction kinetics, which will allow to determine if this cis to trans interconversion is a major cause of the major abundance of trans-4'-OH-PZQ in clinical studies. Overall, caution should be applied when evaluating PZQ pharmacokinetics based on the measurement of trans-4'-OH-PZQ metabolite, as its formation is not only driven by multiple pathways with polymorphic CYPs, but also through a non-CYP interconversion from cis-4'-OH-PZQ.

In a second step, turnover in selected rhCYPs for R-PZQ, S-PZQ and rac-PZQ was determined (Figure 4). Comparison of CLint values between individually tested PZQ enantiomers (100% e.r.) pointed out that R-PZQ is a preferred substrate over S-PZQ for CYP 1A1, 1A2, 2C9 and 2D6, whereas S-PZQ is preferred over R-PZQ for CYP 3A7 (Table S4). Abundant CYP isoforms 3A4, 3A5, as well as 2C19, presented similar efficiency in metabolizing both PZQ enantiomers.

Determination of Michaelis Menten parameters ($K_m$ and $V_{max}$) resulted in a better characterization of the differences between PZQ enantiomers (Figure 5-6). Given that some rhCYPs can generate several PZQ

DMD Fast Forward. Published on March 19, 2020 as DOI: 10.1124/dmd.119.089888
This article has not been copyedited and formatted. The final version may differ from this version.



metabolites with different kinetic parameters (Wang et al., 2014), and that some metabolites are interconverted, kinetic evaluation was pursued following substrate depletion. For CYP 2C9, 3A4 and 3A5, an apparent concomitant affinity increase (lower $K_m$) and rate decrease (lower $V_{max}$) was observed for both enantiomers when assayed as racemate. For CYP 2C19, this effect was only noted for R-PZQ. As both kinetic values changed in the same direction (increase or decrease), the resulting $V_{max}/K_m$ ratio of single enantiomers (i.e. 100% e.r.) was similar to $V_{max}/K_m$ ratio of each enantiomer tested in a racemic mixture (i.e. 50% e.r.) and comparable as well to the $CL_{int}$ of PZQ enantiomers tested at 1.0 µM (Figure S6).

Moreover, by comparing our data with available literature data obtained via metabolite formation (Li et al., 2003; Wang et al., 2014), $K_m$ values obtained following substrate depletion approach were > 2-fold lower for CYP 1A2, 2C19 and 3A4 whilst being similar for 2C9 This could indicate an underestimation of the $K_m$ values by measuring metabolite formation when multiple pathways for the same CYP are involved (Figure 1). Moreover, $K_m$ and $V_{max}$ values obtained for the same enzyme vary considerably within the same study depending on the product measured (Li et al., 2003).

Comparison of kinetic parameters of PZQ enantiomers whether tested individually or as racemate were the basis to select which rhCYPs might be subject to enantiomer-enantiomer interactions. Generally, for these substrate depletion-based inhibition experiments, our recommendation is to use a broad range of concentrations in the assay (whenever possible) to cover all parts of the substrate depletion sigmoidal shape. Although in our case it was possible to adjust concentration ranges to the analytical limitations without impacting the quality of the final estimates, our expectation is that the uncertainty (SD) can be reduced if both plateaus are included. For subsequent data analysis, two approaches were assessed to calculate $K_m$, $V_{max}$ and $K_i$ values all at once, namely a linear static and non-linear dynamic modeling. For both tested modeling approaches, it was concluded that the data from incubations of PZQ enantiomer mixtures with CYP 2C9, 2C19, 3A4 and 3A5 were best fitted using models of competitive inhibition between the enantiomers. Comparison of $K_i$ values between PZQ enantiomers generally resulted in differences below 2-fold, except for CYP 2C19, where Ki was lower for S-PZQ (Table S8-9), potentially indicating that S-PZQ is prevalently playing an inhibitor role. S-PZQ seems as well to act as perpetrator of CYP 1A1 mediated metabolism of R-PZQ, however further experiments are required to confirm the inhibition mechanism.

DMD Fast Forward. Published on March 19, 2020 as DOI: 10.1124/dmd.119.089888
This article has not been copyedited and formatted. The final version may differ from this version.



Numerical differences were expected between the two modeling approaches, because linear static modeling obviates the metabolism of the item defined as inhibitor in the evaluation and in PZQ case study this was not negligible. However, both methods lead to similar numerical values. Even including substrate depletion of both enantiomers, non-linear dynamic modelling only resulted in slightly tighter inter-assay deviations. Thus, the static modeling approach seems to suffice to get a rough estimate of the $K_i$ values for PZQ. However, more case studies are needed to confirm that linear static modeling is sufficient to provide good estimates for concomitant drugs both being metabolized to a relevant degree. Attempts of fitting a linear static mixed model resulted in similar kinetic values as for competitive models but with high variability on alpha estimates.

In order to explore the possibility that the kinetic parameters determined above might explain the different PK behavior between R- and S-PZQ, the generation of PBPK models for each enantiomer, including *in vitro* to *in vivo* extrapolation of the metabolism data reported in this study, was investigated. Several approaches were applied for the in vitro to in vivo extrapolation of the metabolism data obtained using hHeps and rhCYPs, including the standard ISEF approach (Proctor et al., 2004) and an approach involving calibration with reference compounds. The simulated oral clearance for R-PZQ was significantly in under-predicted all cases, in both racemic and R-PZQ ODT formulations (data not shown). The inability to recover in vivo clearance from in vitro data, the erratic shapes of the PK profiles (Bonate et al., 2018), multiple peaks, the large PK variability and the unexplained dose non-linearity of the observed PK (Bagchus et al., 2019) made PBPK model building and parameterization challenging. In light of these complexities, combined with the absence of published data concerning the absolute bioavailability and mass balance of PZQ enantiomers, it would be difficult to fully verify a PBPK model developed from the available *in vitro* and clinical data.

In conclusion, competitive inhibition between PZQ enantiomers was determined in vitro, based on multiple substrate depletion measurements. An abundant CYP 3A4 metabolite found in previous studies was structurally characterized. Moreover, we have shown that, in addition to the multiple metabolic pathways, interconversion between metabolites in hHeps occurs, which could partially explain the human metabolic profile.

## Acknowledgments

The authors gratefully acknowledge Ralf-Erwin Licht and Axel-Walter Thomasberger for their excellent experimental contribution on metabolite profiling and purification, respectively and Dr Vilmos Posevitz

for editorial help. We are also very grateful to Dr. Ulrike Gradhand, Dr. Katrin Georgi, Dr. Wilhelmina Bagchus, Dr. Peter Ballard and Dr. Sheila Annie-Peters for useful discussions and support of the work described here.

## Authorship Contributions

Participated in research design: Vendrell-Navarro, Scheible, Abla, Perrin.

Conducted experiments: Vendrell-Navarro.

Performed data analysis: Vendrell-Navarro, Scheible, Lignet, Marx, Burt.

Wrote or contributed to the writing of the manuscript: Vendrell-Navarro, Scheible, Lignet, Abla, Luepfert, Marx, Burt, Swart, Perrin.

## References

Bagchus WM, Bezuidenhout D, Harrison-Moench E, Kourany-Lefoll E, Wolna P, and Yalkinoglu O (2019) Relative Bioavailability of Orally Dispersible Tablet Formulations of Levo- and Racemic Praziquantel: Two Phase I Studies. *Clinical and translational science* **12:**66-76.

Bonate PL, Wang T, Passier P, Bagchus W, Burt H, Lüpfert C, Abla N, Kovac J, and Keiser J (2018) Extrapolation of praziquantel pharmacokinetics to a pediatric population: a cautionary tale. *Journal of Pharmacokinetics and Pharmacodynamics* **45:**747-762.

Dandara C, Ballo R, and Parker MI (2005) CYP3A5 genotypes and risk of oesophageal cancer in two South African populations. *Cancer letters* **225:**275-282.

Dandara C, Lombard Z, Du Plooy I, McLellan T, Norris SA, and Ramsay M (2011) Genetic variants in CYP (-1A2, -2C9, -2C19, -3A4 and -3A5), VKORC1 and ABCB1 genes in a black South African population: a window into diversity. *Pharmacogenomics* **12:**1663-1670.

FDA (1992) FDA'S policy statement for the development of new stereoisomeric drugs. *Chirality* **4:**338-340.

Fernandez P, Zeigler-Johnson CM, Spangler E, van der Merwe A, Jalloh M, Gueye SM, and Rebbeck TR (2012) Androgen Metabolism Gene Polymorphisms, Associations with Prostate Cancer Risk and Pathological Characteristics: A Comparative Analysis between South African and Senegalese Men. *Prostate cancer* **2012:**798634.

Fowler S and Zhang H (2008) In Vitro Evaluation of Reversible and Irreversible Cytochrome P450 Inhibition: Current Status on Methodologies and their Utility for Predicting Drug–Drug Interactions. *AAPS J* **10:**410-424.

Huang J, Bathena SPR, and Alnouti Y (2010) Metabolite Profiling of Praziquantel and its Analogs During the Analysis of in vitro Metabolic Stability Using Information-Dependent Acquisition on a Hybrid Triple Quadrupole Linear Ion Trap Mass Spectrometer. *Drug Metabolism and Pharmacokinetics* **25:**487-499.

Jamei M, Marciniak S, Edwards D, Wragg K, Feng K, Barnett A, and Rostami-Hodjegan A (2013) The simcyp population based simulator: architecture, implementation, and quality assurance. *In Silico Pharmacol* **1:**9-9.

Jamei M, Turner D, Yang J, Neuhoff S, Polak S, Rostami-Hodjegan A, and Tucker G (2009) Population-based mechanistic prediction of oral drug absorption. *AAPS J* **11:**225-237.

Jones HM and Houston JB (2004) Substrate depletion approach for determining in vitro metabolic clearance: time dependencies in hepatocyte and microsomal incubations. *Drug Metabolism and Disposition* **32:**973.

Kong D, Li Q, Zhang P, Zhang W, Zhen Y, and Ren L (2015) The truth about the lower plasma concentration of the (−)-isomer after racemic doxazosin administration in rats: Stereoselective inhibition of the (−)-isomer by the (+)-isomer at CYP3A. *European Journal of Pharmaceutical Sciences* **77:**238-245.

Kuehl P, Zhang J, Lin Y, Lamba J, Assem M, Schuetz J, Watkins PB, Daly A, Wrighton SA, Hall SD, Maurel P, Relling M, Brimer C, Yasuda K, Venkataramanan R, Strom S, Thummel K, Boguski MS, and Schuetz E (2001) Sequence diversity in CYP3A promoters and characterization of the genetic basis of polymorphic CYP3A5 expression. *Nature genetics* **27:**383-391.

Li X-Q, Björkman A, Andersson TB, Gustafsson LL, and Masimirembwa CM (2003) Identification of human cytochrome P450s that metabolise anti-parasitic drugs and predictions of in vivo drug hepatic clearance from in vitro data. *European Journal of Clinical Pharmacology* **59:**429-442.

Ludden TM, Beal SL, and Sheiner LB (1994) Comparison of the Akaike Information Criterion, the Schwarz criterion and the F test as guides to model selection. *Journal of Pharmacokinetics and Biopharmaceutics* **22:**431-445.

Melo AJB, Iamamoto Y, Maestrin APJ, Smith JRL, Santos MD, Lopes NP, and Bonato PS (2005) Biomimetic oxidation of praziquantel catalysed by metalloporphyrins. *Journal of Molecular Catalysis A: Chemical* **226:**23-31.

Meyer T, Sekljic H, Fuchs S, Bothe H, Schollmeyer D, and Miculka C (2009) Taste, A New Incentive to Switch to (R)-Praziquantel in Schistosomiasis Treatment. *PLOS Neglected Tropical Diseases* **3:**e357.

Nath A and Atkins WM (2006) A Theoretical Validation of the Substrate Depletion Approach to Determining Kinetic Parameters. *Drug Metabolism and Disposition* **34:**1433.

Nleya L, Thelingwani R, Li XQ, Cavallin E, Isin E, Nhachi C, and Masimirembwa C (2019) The effect of ketoconazole on praziquantel pharmacokinetics and the role of CYP3A4 in the formation of X-OH-praziquantel and not 4-OH-praziquantel. *Eur J Clin Pharmacol* **75:**1077-1087.

Obach RS and Reed-Hagen AE (2002) Measurement of Michaelis constants for cytochrome P450-mediated biotransformation reactions using a substrate depletion approach. *Drug Metab Dispos* **30:**831-837.

Patzschke K, Putter J, Wegner LA, Horster FA, and Diekmann HW (1979) Serum concentrations and renal excretion in humans after oral administration of praziquantel--results of three determination methods. *European journal of drug metabolism and pharmacokinetics* **4:**149-156.

Proctor NJ, Tucker GT, and Rostami-Hodjegan A (2004) Predicting drug clearance from recombinantly expressed CYPs: intersystem extrapolation factors. *Xenobiotica* **34:**151-178.

Sjögren E, Lennernäs H, Andersson TB, Gråsjö J, and Bredberg U (2009) The multiple depletion curves method provides accurate estimates of intrinsic clearance (CLint), maximum velocity of the metabolic reaction (Vmax), and Michaelis constant (Km): accuracy and robustness evaluated through experimental data and Monte Carlo simulations. *Drug Metabolism and Disposition* **37:**47-58.

Stothard JR, Sousa-Figueiredo JC, Betson M, Green HK, Seto EY, Garba A, Sacko M, Mutapi F, Nery SV, and Amin MA (2011) Closing the praziquantel treatment gap: new steps in epidemiological monitoring and control of schistosomiasis in African infants and preschool-aged children. *Parasitology* **138:**1593-1606.

Wang H, Fang Z-Z, Zheng Y, Zhou K, Hu C, Krausz KW, Sun D, Idle JR, and Gonzalez FJ (2014) Metabolic profiling of praziquantel enantiomers. *Biochemical Pharmacology* **90:**166-178.

Wood FL, Houston HJ, Hallifax D (2017). Clearance Prediction Methodology Needs Fundamental Improvement: Trends Common to Rat and Human Hepatocytes/Microsomes and Implications for Experimental Methodology. Drug Metabolism and Disposition. 45: p. 1178 - 1188.

WHO (2007) BL 6. Business Plan. 2008-2013. Drug development and evaluation for helminths and other neglected tropical diseases, in: *Draft Business Plan for JCB*, pp 18-19, Research&Training in Tropical Diseases (TDR).

WHO (2009) WHO model formulary 2008 (Marc C. Stuart MK, Suzanne R. Hill. ed, Geneva.

WHO (2010) Drug development and evaluation for helminths and other neglected tropical diseases - 2009 annual report (TDR/BL6.10 ed, pp 28-29.

WHO (2018) Schistosomiasis Fact sheet number 115. http://www.who.int/en/news-room/fact-sheets/detail/schistosomiasis.

## Footnotes

Not applicable.

DMD Fast Forward. Published on March 19, 2020 as DOI: 10.1124/dmd.119.089888
This article has not been copyedited and formatted. The final version may differ from this version.



## Figure legends

**Figure 1. Transformation pathway of PZQ mono-oxidations in hHeps.**

If oxidation site is not confirmed, potential oxidation sites are indicated with a gray circle in the metabolite structure. Both R- and S-PZQ are metabolized to cis-4'-OH-PZQ (M4), trans-4'-OH-PZQ (M2), M5 and the herein characterized M6 structure with its oxidation site at carbon-11b. Enantioselective transformations, i.e. M3 for R-PZQ and M1 for S-PZQ, are represented at left and right side, respectively. Moreover, the proposed enzymatic cis- to trans conversion occurring in hHeps is illustrated.

**Figure 2. Relative abundance of the mono-oxidation metabolites of R- and S-PZQ formed in rhCYPs, HLM and hHeps.**

Mono-oxidation metabolites are represented in different format and arranged along the z-axis. Relative abundance of metabolite is given by the total MS peak area (%) and scaled over y-axis. Test system (rhCYP isoform, HLM or hHeps) is indicated on the x-axis. For rhCYPs and HLM, values at 30 min incubation time are represented, whereas for hHeps 3 time points are given (30, 90, 180 min).

**Figure 3. Interconversion of cis-4'-OH-PZQ metabolites in hHeps.**

Time-course measurement of all 4'-OH-PZQ metabolites in incubations of R- and S- cis-4'-OH-PZQ with hHeps revealed a cis to trans interconversion.

**Figure 4. In vitro clearance of PZQ enantiomers in the panel of rhCYPs.**

Comparison of $CL_{int}$ between R-PZQ and S-PZQ, either as isolated enantiomer (100% e.r.) or mixed as racemate (50% e.r.). Mean and standard deviation of mean is represented.

**Figure 5. Affinity (as Michaelis-Menten $K_m$ value) of PZQ enantiomers for rhCYPs.**

Mean and standard error of mean are represented. Low clearance cases leading to a CV higher than 80% are considered as non-converged and marked with a "°" sign.

**Figure 6. Turnover rate (as Michaelis-Menten $V_{max}$ value) of PZQ enantiomers mediated by rhCYPs.**

DMD Fast Forward. Published on March 19, 2020 as DOI: 10.1124/dmd.119.089888
This article has not been copyedited and formatted. The final version may differ from this version.



Mean and standard error of mean are represented. Low clearance cases leading to a CV higher than 80% are considered as non-converged and marked with a "°" sign.

**Figure 7. Substrate depletion curve dataset based on the linear static model to determine PZQ enantiomer-enantiomer interactions on CYP 2C19 metabolism.**

DMD Fast Forward. Published on March 19, 2020 as DOI: 10.1124/dmd.119.089888
This article has not been copyedited and formatted. The final version may differ from this version.

## Tables

**Table 1. Determination of interaction kinetics based on linear static model and non-linear dynamic model**

Inter-assay mean and standard error of mean are given (N=2-4), except for CYP3A7 where only N=1 was done. Low clearance cases with an associated CV above 80% are described as not converged (n.c.) and labelled in gray and italic.

| | | **Kinetic values at 100% e.r.** | | **Interaction kinetics based on linear static model** | | | **Interaction kinetics based on dynamic non-linear model** | | |
|---|---|---|---|---|---|---|---|---|---|
| CYP | Test item | $K_m$ [µM] | $V_{max}$ [pmol/pmol CYP/min] | $K_m$ [µM] | $V_{max}$ [pmol/pmol CYP/min] | $K_i$ [µM] | $K_m$ [µM] | $V_{max}$ [pmol/pmol CYP/min] | $K_i$ [µM] |
| 1A1 | R-PZQ | 9.6 ± 2.1 | 46 ± 9 | 7.8 ± 1.6 | 31 ± 3 | *n.c.* | 6.8 ± 4.3 | 25 ± 6 | 23 ± 7 |
| | S-PZQ | *n.c.* | 80 ± 53 | *n.c.* | *n.c.* | 29 ± 0 | 25 ± 8 | 35 ± 27 | 25 ± 3 |
| 2C9 | R-PZQ | 40 ± 25 | 130 ± 90 | 46 ± 10 | 144 ± 13 | 33 ± 15 | 30 ± 3 | 77 ± 8 | 31 ± 8 |
| | S-PZQ | 25 ± 8 | 37 ± 15 | 24 ± 3 | 34 ± 7 | 36 ± 19 | 16 ± 4 | 20 ± 6 | 22 ± 5 |
| 2C19 | R-PZQ | 7.4 ± 1.4 | 42 ± 9 | 8.4 ± 1.0 | 69 ± 20 | 6.9 ± 0.6 | 6.4 ± 1.5 | 40 ± 5 | 9.4 ± 0.4 |
| | S-PZQ | 1.1 ± 0.1 | 8.9 ± 0.6 | 2.7 ± 0.6 | 23 ± 4 | 3.0 ± 1.1 | 2.8 ± 0.4 | 17 ± 1 | 2.4 ± 0.7 |
| 3A4 | R-PZQ | 22 ± 4 | 60 ± 14 | 30 ± 20 | 51 ± 34 | 29 ± 10 | 25 ± 14 | 42 ± 28 | 18 ± 6 |
| | S-PZQ | 26 ± 12 | 78 ± 42 | 24 ± 6 | 63 ± 6 | 21 ± 8 | 24 ± 8 | 36 ± 14 | 21 ± 2 |
| 3A5 | R-PZQ | 57 ± 21 | 92 ± 40 | 20 ± 4 | 34 ± 6 | 39 ± 24 | 22 ± 1 | 28 ± 1 | 27 ± 6 |
| | S-PZQ | 69 ± 28 | 127 ± 49 | 24 ± 2 | 47 ± 6 | 27 ± 4 | 19 ± 5 | 32 ± 4 | 15 ± 1 |
| 3A7 | R-PZQ | *n.c.* | *n.c.* | *n.c.* | *n.c.* | *n.c.* | *n.c.* | *n.c.* | 153 |
| | S-PZQ | 8.1 | 4.5 | 209 | 97 | *n.c.* | 178 | 75 | *n.c.* |

DMD Fast Forward. Published on March 19, 2020 as DOI: 10.1124/dmd.119.089888
This article has not been copyedited and formatted. The final version may differ from this version.

**Table 2. Summary PK parameters based on simulated and observed plasma concentrations following the oral administration of R-PZQ ODTs, and rac-PZQ ODTs.**

Geometric mean (Geometric CV, %) values are reported. Simulations were performed using the $V_{max}$ and $K_m$ in rhCYPs generated by the substrate depletion method to describe metabolism. IVIVE scaling was performed using the reference compound scaling approach. †Experimental $V_{max}$ values were multiplied by 5.5. The observed values were obtained from clinical concentration data using non-compartmental analysis.

| **R-PZQ parameters after administration of R-PZQ ODTs†** | | | | | | |
|---|---|---|---|---|---|---|
| **R-PZQ dose [mg/kg]** | **Simulated** | | | **Observed** | | |
| | **$AUC_{(0,24)}$ [h●ng/mL]** | **$CL_{po}$ [L/h]** | **$C_{max}$ [ng/mL]** | **$AUC_{(0,24)}$ (h●ng/mL]** | **$CL_{po}$ [L/h]** | **$C_{max}$ [ng/mL]** |
| **10** | 205 (70) | 3305 (70) | 78 (74) | 188 (109) | 3091 (93) | 90.9 (93) |
| **20** | 467 (71) | 2882 (72) | 177 (75) | 813 (103) | 1665 (94) | 389 (113) |
| **30** | 694 (69) | 2910 (69) | 264 (74) | 2307 (78) | 924 (71) | 1067 (84) |
| **R-PZQ parameters after administration of rac-PZQ ODTs** | | | | | | |
| **rac-PZQ dose [mg/kg]** | **Simulated** | | | **Observed** | | |
| | **$AUC_{(0,24)}$ [h●ng/mL]** | **$CL_{po}$ [L/h]** | **$C_{max}$ [ng/mL]** | **$AUC_{(0,24)}$ [h●ng/mL]** | **$CL_{po}$ [L/h]** | **$C_{max}$ [ng/mL]** |
| **20** | 1565 (71) | 420 (70) | 553 (68) | 331 (74) | 2157 (63) | 157 (83) |
| **40** | 4033 (71) | 336 (73) | 1432 (66) | 2067 (46) | 697 (44) | 885 (57) |
| **60** | 5853 (75) | 340 (73) | 2142 (72) | 4955 (41) | 435 (45) | 1562 (32) |
| **S-PZQ parameters after administration of rac-PZQ ODTs** | | | | | | |
| **rac-PZQ dose [mg/kg]** | **Simulated** | | | **Observed** | | |
| | **$AUC_{(0,24)}$ [h●ng/mL]** | **$CL_{po}$ [L/h]** | **$C_{max}$ [ng/mL]** | **$AUC_{(0,24)}$ [h●ng/mL]** | **$CL_{po}$ [L/h]** | **$C_{max}$ [ng/mL]** |
| **20** | 1481 (85) | 444 (83) | 532 (80) | 2278 (46) | 313 (47) | 797 (41) |
| **40** | 4116 (87) | 329 (90) | 1476 (78) | 7783 (28) | 185 (32) | 2347 (31) |
| **60** | 5825 (90) | 341 (88) | 2177 (83) | 14832 (34) | 145 (40) | 3263 (20) |

DMD Fast Forward. Published on March 19, 2020 as DOI: 10.1124/dmd.119.089888
This article has not been copyedited and formatted. The final version may differ from this version.

## Figures

**Figure 1. Transformation pathway of PZQ mono-oxidations in hHeps.**

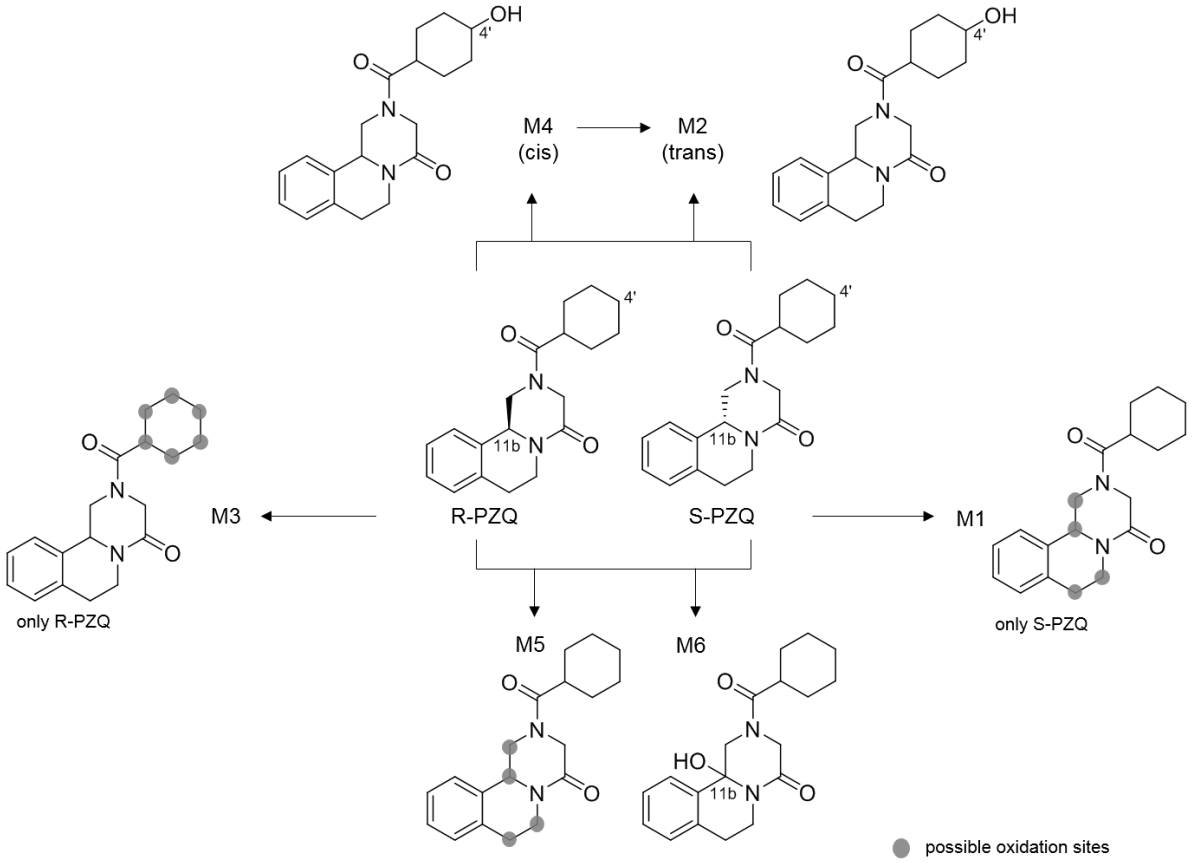

DMD Fast Forward. Published on March 19, 2020 as DOI: 10.1124/dmd.119.089888
This article has not been copyedited and formatted. The final version may differ from this version.

**Figure 2. Relative abundance of the mono-oxidation metabolites of R- and S-PZQ formed in rhCYPs, HLM and hHeps.**

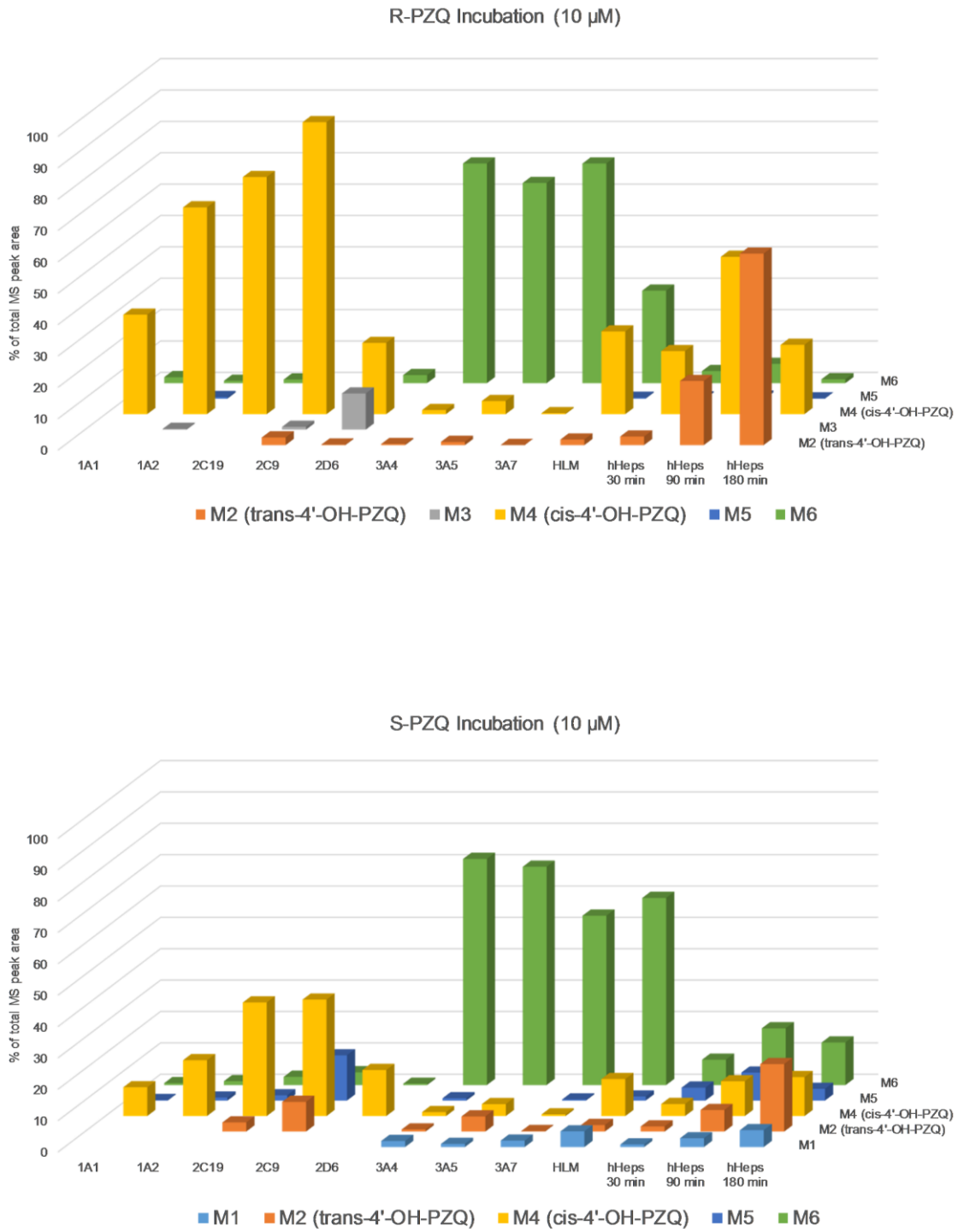

DMD Fast Forward. Published on March 19, 2020 as DOI: 10.1124/dmd.119.089888
This article has not been copyedited and formatted. The final version may differ from this version.

**Figure 3. Interconversion of cis-4'-OH-PZQ metabolites in hHeps.**

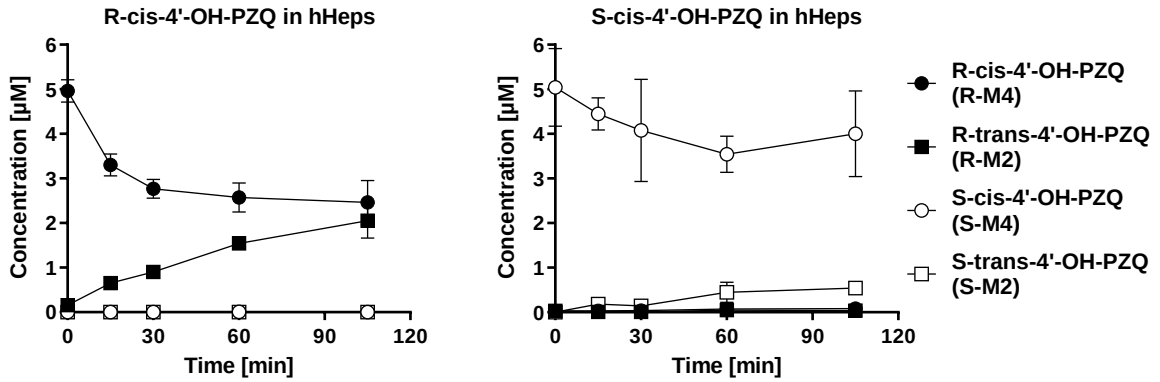


**Figure 4. In vitro clearance of PZQ enantiomers in the panel of rhCYPs.**

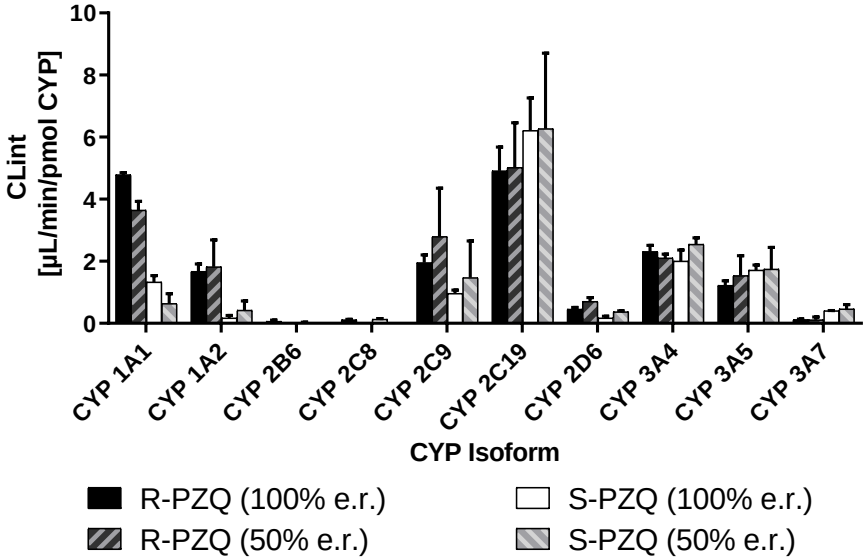

DMD Fast Forward. Published on March 19, 2020 as DOI: 10.1124/dmd.119.089888
This article has not been copyedited and formatted. The final version may differ from this version.

**Figure 5. Affinity (as Michaelis-Menten $K_m$ value) of PZQ enantiomers for rhCYPs.**

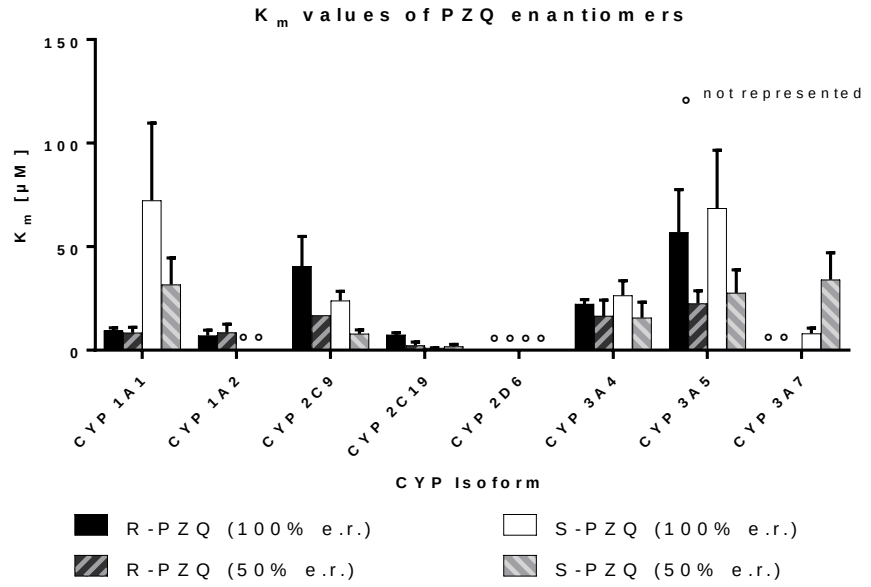


**Figure 6. Turnover rate (as Michaelis-Menten $V_{max}$ value) of PZQ enantiomers mediated by rhCYPs**

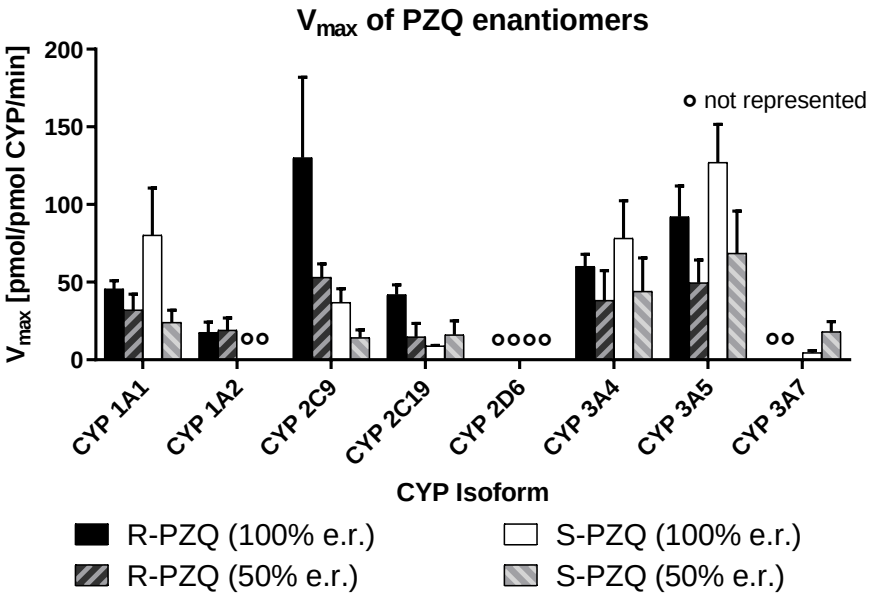


**Figure 7. Substrate depletion curve dataset based on the linear static model to determine PZQ enantiomer-enantiomer interactions on CYP 2C19 metabolism.**

DMD Fast Forward. Published on March 19, 2020 as DOI: 10.1124/dmd.119.089888
This article has not been copyedited and formatted. The final version may differ from this version.